Investigation on the Flow Field Characteristics of a Highly Underexpanded Pulsed Plasma Jet

Jong-Uk Kim*
Center for Advanced Accelerators, Korea Electrotechnology Research Institute 28-1 Seongju-dong, Changwon 641-120, Korea
Youn J. Kim
School of Mechanical Engineering Sungkyunkwan University 300 Chunchun-dong, Suwon, Kyunggi-do 440-746, Korea

In recent years, significant progress has been made in modeling turbulence behavior in plasma and its effect on transport. It has also been made in diagnostics for turbulence measurement; however, there is still a large gap between theoretical model and experimental measurements. Visualization of turbulence can improve the connection to theory and validation of the theoretical model. One method to visualize the flow structures in plasma is a laser Schlieren imaging technique. We have recently applied this technique and investigated the characteristics of a highly underexpanded pulsed plasma jet originating from an electrothermal capillary source. Measurements include temporally resolved laser Schlieren imaging of a precursor blast wave. Analysis on the trajectory of the precursor blast wave shows that it does not follow the scaling expected for a strong shock resulting from the instantaneous deposition of energy at a point. However, the shock velocity does scale as the square root of the deposited energy, in accordance with the point deposition approximation.

Key Words : Plasma Jet, Mach Disk, Blast Wave, Schlieren Imaging

1. Introduction

Recently, electrothermal plasma injection has been suggested as a means to enhance and control combustion rate of propellant materials. Electrothermal plasmas are also of interest for applications such as rocket propulsion, electrothermal-chemical launchers, and hypersonic mass acceleration technology (Hewkin and Figura, 1993; Greig *et al.*, 1993). Electrothermal-chemical (ETC) gun propulsion uses a pulsed power system to generate a plasma, which is then injected into a chemical propellant to improve gun performance, control, and safety of gun systems (Schmidt et al., 1975; Kaplan *et al.*, 1993; Gilligan *et al.*, 1991). In an ETC gun, an electrical energy pulse is first converted to the thermal and kinetic energy of a plasma, and the plasma energy is used to ignite the chemical propulsion charge (e.g., solid propellant) as well as to enhance gun performance by taking advantage of a number of unique plasma characteristics. For example, a low density plasma jet can efficiently ignite charges of high loading density and control propellant mass generation rates (Del Guercio, 1997). In addition, it can reduce propellant charge temperature sensitivity, i.e. , the variation of gun performance with changing ambient temperature (Dyvik et al., 1996), and can shorten ignition delay. Plasma igniters also eliminate the problems of conventional chemical igniter and thus can enhance the safety aspects of a overall

* Corresponding Author,
E-mail : jukim@keri.re.kr
TEL : +82-55-280-1462; **FAX** : +82-55-280-1469
Center for Advanced Accelerators Korea Electrotechnology Research Institute(KERI), 28-1 Seongju-dong, Changwon, Kyungnam 641-120, Korea. (Manus-ript **Received** February 6, 2001; **Revised** September 25, 2001)

gun propulsion system. All these aspects have a significant influence on the ballistics of ETC gun systems and can lead to a useful improvement in gun performance and accuracy.

In many proposed ETC gun systems the plasma ignites a solid propellant charge; the total energy may also be augmented by plasma injection into the gun chamber and/or the barrel. Despite the demonstrated improvements in gun performance using ETC propulsion, little is currently known about the fundamental processes involved in plasma-initiated combustion of a solid propellant. In fact, little is known of the characteristics of the electrothermal plasma itself. Major unknowns in ignition, reaction rates and plasma jet surface geometry attribute to this complex energetic mixing process. The present level of modeling of reactive plasma-fluid interaction is preliminary and largely unverified. Therefore, detailed diagnostic test data for the plasma-working fluid behavior is needed. Understanding the control of combustion events by thermal input from an electrically driven plasma system will offer a fundamental challenge to fluids and thermal technology both from the experimental perspective and the computational modeling of the phenomena involved. From this point of view, fundamental studies such as optical emission spectroscopy (OES) and flow structures on plasma jet are necessary to provide better understanding of the chemical or physical phenomena involved within the plasma jet.

Previous work has shown that the capillary discharge produced a transient highly underexpanded plasma jet that lasted for about 250 μs (Kohel *et al.*, 1998). The present work is a continuation of the work reported in Kohel *et al.* (1998), where preliminary optical emission spectroscopic measurements were made for a limited range of experimental conditions for evaluation of the compositions of the species, electron temperature and number density in a plasma jet.

The main objective of the present work, therefore, is to investigate the physical characteristics of flow structure of a pulsed polycarbonate capillary plasma jet that is allowed to expand freely into the room atmosphere. In order to investigate the evolution of flow structure of the plasma jet, temporally resolved visible emission imaging with a gated intensified CCD camera and temporally resolved Schlieren imaging technique are employed in this study.

2. Experimental Approach

2.1 Design and operation of the pulsed plasma source

A schematic diagram of the experimental arrangement is shown in Fig. 1. The plasma source is generated by rapid discharge of 3.1 kJ of electrical energy into a polycarbonate (Lexan) capillary. This energy is stored in a 251 μF capacitor charged to a maximum of 5 kV. The capillary is 3 mm in diameter, 30 mm long, and is open at one end only. The discharge is initiated with a thin copper fuse wire (64 μm) and ablation and ionization of material from the capillary surface sustains the discharge. The resulting plasma rapidly expands from the open end of a capillary and issues into room air. The peak current through the plasma is approximately 4.6 kA for discharge energy of 3.1 kJ, and the discharge duration is approximately 250 μs. The electrodes are made of a copper-tungsten alloy (30% Cu, 70% W) to resist electrode erosion. The voltage across the capillary is measured as a function of time using a high voltage probe (Tektronics P6015A). The current trace is measured using a Rogowski coil and the signal is integrated with respect to time to get the total current in the plasma circuit during the discharge. The Rogowski coil (Knoepfel, 1970) is magnetically coupled to the current through the major loop of the toroid. The induced output voltage u of the Rogowski coil with W turns, average toroidal circumstance L, and single turn cross-sectional area S, is directly proportional to the time rate of change of the total current I of loop passing through the toroid,

$$u=[WS\mu_0/L]\times[dI(t)/dt] \quad (1)$$

Where μ_0 is the permeability of free space. From Eq. (1), it is clear that the Rogowski coil is equivalent to a current differentiator. Therefore,

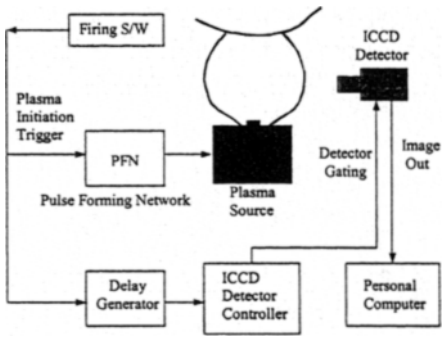

Fig. 1 Schematic diagram of experimental setup for acquiring emission images and temporally- and spatially- resolved spectra of the plasma jet

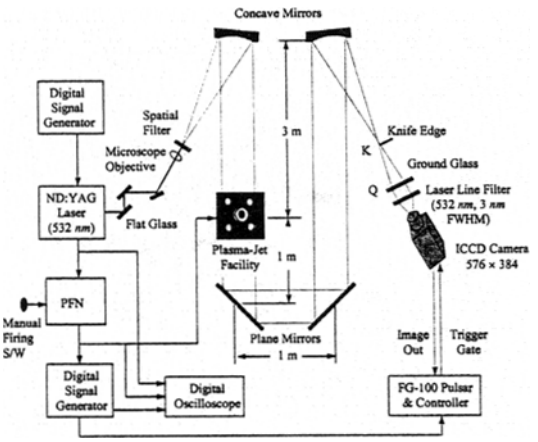

Fig. 2 Schematic diagram of the experimental setup for Schlieren imaging of the plasma jet

an activate integrator is added at the output terminal of the coil, yielding a voltage proportional to the current. The measured voltage and current waveforms are highly repeatable, for example, the peak current is repeatable to less than 3%.

2.2 Optical system for schlieren imaging of the plasma jet

The Schlieren imaging is a well-established technique that enables visualization of the index-of-refraction gradients in a flow field. Figure 2 shows a schematic diagram of the Schlieren imaging system used in this study. The second harmonic (532 nm) of a pulsed Nd:YAG laser was used as a light source. The pulse duration was 10 ns, which was sufficient to freeze the motion of flow. To improve image quality the beam was spatially filtered by passing it through a 25×microscope objective lens, which focused the beam onto a 25 μm pinhole. The laser pulse was first attenuated (to about 5 μJ per pulse) by reflecting it from three flat glasses to avoid burning the pinhole. The spatial filter was placed at the focus of a concave mirror, so that the working section was fully illuminated by a collimated beam of light. To protect the camera from damage, the Schlieren image was projected onto a ground glass target (50 mm×50 mm×1.6 mm). The target was imaged using an intensified CCD camera (Princeton Instruments ICCD-576, 576×384 pixel resolution) fitted with a 105 mm focal length (AF Micro Nikkor) camera lens operated at $f/22$. To reduce interference from intense emission from the plasma jet, a laser line filter (532 nm, 3 nm bandwidth) was placed in front of the camera lens. To further reduce the background luminosity from the plasma, the second Schlieren mirror was placed approximately 6 m from the plasma source.

2.3 Overall synchronization

One problem in conducting the Schlieren imaging is to obtain a laser pulse at any desired time delay from initiation of the discharge. Since the laser is inherently a synchronous device that operates at 10 Hz, it cannot be fired at an arbitrary time. A further complication is that the laser requires the flash lamps being triggered 165 μs before the Q-switch (which initiates the laser pulse). Our solution is to build a triggering circuit that, upon the input of a manual trigger, would initiate the discharge at a user-set time *before* the next laser pulse is to be fired. Since there is a relatively short time delay between the triggering physical beginning (about 6 μs) of the discharge, and the discharge itself is over in about 250 μs, these triggering events easily take place within 100 ms between the 10 Hz laser pulses. The ICCD camera is synchronized with the laser to insure that a laser pulse occurrs during the 280 ns gate width (i. e. integration time) of the camera. Only one image is taken per laser shot

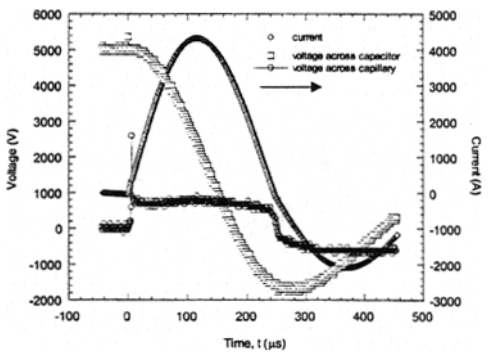

Fig. 3 Typical voltage and current traces obtained during a firing of the plasma jet for an initial capacitor voltage of 5.0 kV

with this configuration, and the acquired Schlieren images are transferred to computer memory for further analysis.

3. Results and Discussions

3.1 Current, voltage and capillary erosion measurements

Figure 3 represents typical voltage and current traces obtained during a discharge with an initial capacitor voltage of 5.0 kV. The figure shows the current, the voltage across the capacitor, and the voltage across the capillary. When the discharge is triggered (by closing an ignition switch), the voltage across the capacitor decreases rapidly and the voltage across the capillary increases. If t is the time elapsed from triggering of the discharge, a peak voltage of 2.6 kV is induced across the capillary over an interval $0\ \mu s < t \leq 6\ \mu s$. A relatively constant voltage ($\leq 1\ kV$) is observed for $t > 6\ \mu s$ and lasts until $t \sim 250\ \mu s$. The initial transient voltage spike occurs just prior to the explosion of the copper wire and the plasma initiation begins after that time, i. e., the high discharge current causes the fuse wire to break down within 6 μs. For the 5 kV case the capacitor is completely discharged in about 250 μs, and the current reaches a peak value of 4.6 kA at 115 μs after the start of the discharge.

The explosion of the copper wire provides a conducting vapor, and subsequent ablation and ionization of dielectric material from the capillary

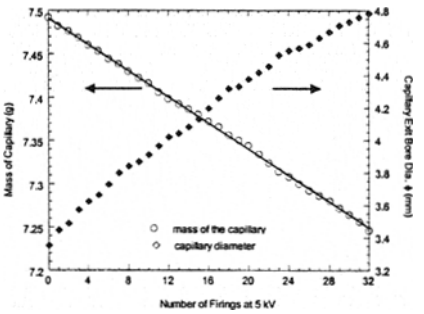

Fig. 4 Changes of the capillary exit diameter and mass with respect to number of firings

walls maintain the plasma within the capillary as the plasma jet discharges into the atmosphere. The increase of the capillary exit diameter (ϕ) due to the erosion of the capillary bore is shown in Fig. 4. Note that the diameter is measured only at the bore exit, but it is known that the capillary does not erode uniformly, i. e. its diameter is not constant along its length. From Fig. 4 we observe that the mass of the capillary decreases approximately linearly with the number of shots. A least-squares fit to the data shows that approximately 7. 6 mg of the capillary is ablated for each firing.

3.2 Flow structure of the plasma-jet

The plasma jet ejected from the open end of the capillary forms a highly under-expanded jet with a characteristic barrel shock structure. In a previous study (Kohel *et al.*, 1998), time-resolved visible emission images of the plasma jet were obtained using an ICCD detector. A representative image taken at 94 μs after initiation of the discharge is shown in Fig. 5, with a schematic description of notable features of quasi-steady free jet flow. Expansion waves at the bore exit travel to the jet boundary where they are reflected to form weak compression waves, which then coalesce into a barrel shock. The barrel shock undergoes an irregular reflection and, in the triple-point downstream from the bore exit, the reflected shock, Mach disk, and slip surface are formed (Liepmann et al., 1957; Christ et al., 1966; Abbet, 1971; Eggins and Jackson, 1974). Here the slip surface represents the surface to separate subsonic

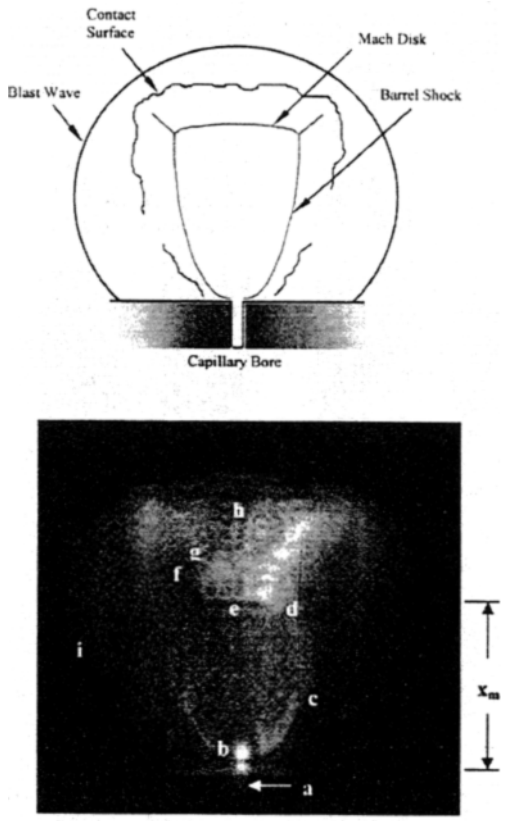

Fig. 5 Schematic diagram of principal features of a quasi-steady free jet (above). Short duration (250 *ns*) image of plasma jet emission, where (a) exit bore, (b) Prandtl-Meyer expansion (Mach cone), (c) barrel shock, (d) Triple-point, (e) Mach disk, (f) Reflected shock, (g) Slip surface, (h) Contact surface, and (i) Jet boundary, respectively; Xm is the Mach disk location

core stream tube from supersonic outer flow downstream of the Mach disk. In the shock-bounded, highly underexpanded jet flow region, the flow is characterized by relatively high Mach numbers ($M \gg 1$), low pressures, and low temperatures. Across the Mach disk, the flow is decelerated to subsonic velocity, the pressure is suddenly increased to atmospheric pressure or above, and the temperature is also increased due to shock heating at the Mach disk.

3.3 Schlieren imaging of the blast wave

Figures 6(a) and 6(b) show six sequential Schlieren images of the expanding plasma jet for initial voltages of 2.5 kV (0.78 kJ) and 5 kV (3.1 kJ), respectively. About 30 μs after plasma initiation, the blast wave expands from the bore exit of the capillary. The blast wave development is an unsteady process comparable to the shock propagation from the open end of a shock tube or from the barrel of a rifle (Klingenberg and Heimerl, 1992). As in the shock tube flow, a nearly spherical shock wave develops, the expansion region immediately adjacent to the bore exit is a Prandtl-Meyer expansion. The flow expansion is initially restrained by the outer blast wave. It is interesting to note that the index-of-refraction gradients are so large across the blast wave that they completely mask the barrel shock inside it.

The radius R of the shock, which is assumed to be the distance from the bore exit to the shock measured along the capillary axis, is measured as a function of time. This is justified by our observation that the position of the shock is highly repeatable from shot-to-shot. For example, four Schlieren images were taken at time $t = 50$ μs (5 kV initial voltage) and the average value of R was found to be 32.7 mm with a standard deviation of 0.10 mm. Shock trajectory measurements were made for image sequences obtained for initial capacitor voltages of 2.5 kV [Fig. 6(a)], 3.5 kV (not shown) and 5 kV [Fig. 6(b)]. The variations of shock trajectories for all three voltages are shown in Fig. 7. The dashed line represents a linear fit for the case of 5.0 kV plasma discharge. Wilson *et al.* (1999) scaled the blast wave trajectories scale as $R \sim t^{(2+\beta)/5}$, where β was a parameter related to the rate of energy deposition (Dabora, 1972). Instantaneous energy deposition corresponds to $\beta=0$, i. e. $R \sim t^{2/5}$, which is a strong spherical shock solution (Taylor, 1950; Sakurai, 1964). The approximately first power dependence of R on t observed experimentally, corresponds to $\beta=3$. Dashed lines corresponding to $\beta=0$ and $\beta=2$ are also shown on Fig. 7. Because energy is being deposited continuously during the discharge it is

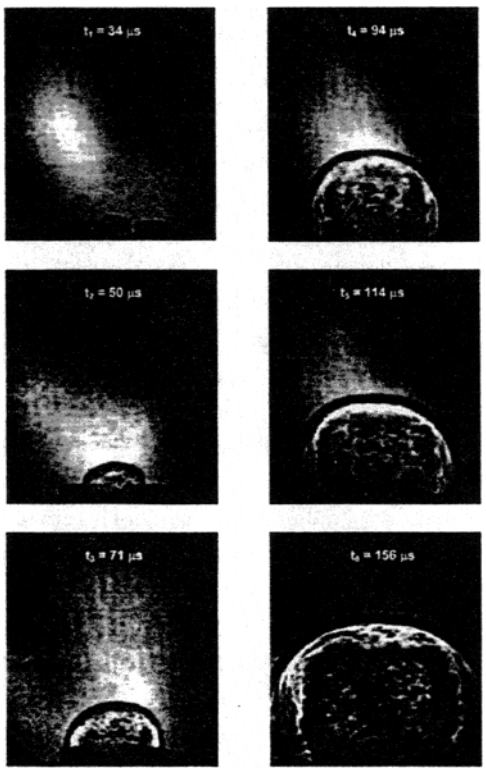

Fig. 6(a) Schlieren image of plasma jet from 2.5 kV discharge

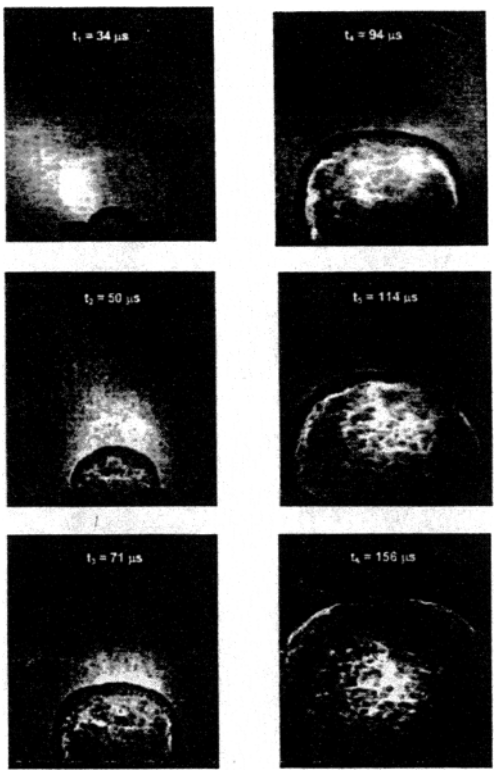

Fig. 6(b) Schlieren image of plasma jet from 5.0 kV discharge

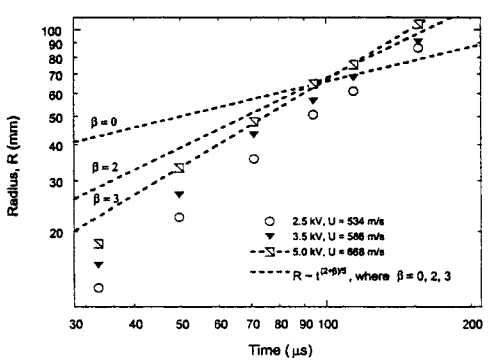

Fig. 7 Experimental data for time-dependence of blast wave radius (R) for three discharge conditions. The dashed line is a linear fit to the 5.0 kV discharge data. This corresponds to energy deposition rate parameter, $\beta=3$ (see text). Other lines correspond to $\beta=0$ (instantaneous energy deposition, $R\propto t^{2/5}$) and $\beta=2$

unsurprising that the $\beta=0$ line does not match the data. The $\beta=2$ line is shown for comparison with computations of Kim and Wilson (1999).

From the blast wave trajectories shown in Fig. 7 it can be seen that the shock velocities are approximately constant with values of 668, 586, and 534 m/s for charging voltages of 5.0, 3.5, and 2.5 kV, respectively. A plot of the blast wave velocity vs. the square root of initial electrical energy ($E^{1/2}$) is shown in Fig. 8. The dashed line is the fit to the data. This shows that the velocity of the blast wave is approximately proportional to $E^{1/2}$. From the emission images of Kohel *et al.* (1999), the contact surface (CS) and Mach disk (MD) locations are measured and those results combined with the blast wave position data are shown in Fig. 9. The additive lines are the theoretical calculations of Kim and Wilson (1999) using the model of Wilson *et al.* (1999) for the Mach disk and contact surface and for the blast wave (BW) approximation, respectively. One can observe a good agreement between the cal-

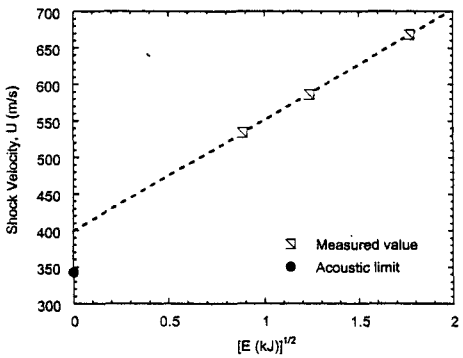

Fig. 8 Dependence of blast wave velocity on initial electrical energy.

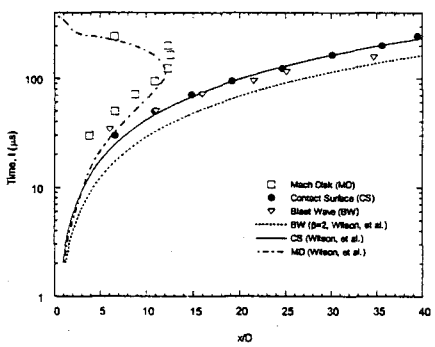

Fig. 9 Experimental axial trajectories (symbols) of the blast wave (BW), contact surface (CS) and Mach disk (MD) and comparison with computations of Kim and Wilson (1999) for $\beta=2$.

culations and measurements for the Mach disk and contact surface, but there is a bigger difference in the blast wave trajectory. In the theoretical model, Kim and Wilson (1999) use $\beta=2$, to account for continuous energy deposition. Earlier calculations with $\beta=0$ showed still larger discrepancy with our experimental observations. As noted above, Fig. 7 shows that our blast wave velocity data are more consistent with $\beta=3$, and computations of blast wave trajectories with this value would agree better with the experiment. The axial displacement histories (see Fig. 9) show that the Mach disk and the contact surface move continuously away from the bore exit of the plasma jet until they attain a maximum standoff. Then the direction of the motion is reversed, and the Mach disk retreats upstream towards the capillary. Figure 9 also shows that the axial motions of the blast wave and the contact surface are closely coupled for a relatively long time. The blast wave and contact surface appears to separate some time after 70 μs, with the blast wave moving slightly faster than the contact surface. There is clear separation 160 μs after plasma initiation. During the interval $0\ \mu s \leq t \leq 160\ \mu s$ the blast wave appears to restrain the flow expansion. At $t=160\ \mu s$ the Mach disk attains its maximum axial distance from the exit. Subsequently, it retreats back toward the bore exit owing to the decrease of the capillary bore pressure as the discharge terminates.

4. Conclusions

In this study, we have made temporally resolved Schlieren imaging of blast shock wave of a pulsed plasma jet produced by a capillary discharge issuing into room air. Trajectories of the blast wave from the pulsed plasma jet were measured at discharge energies of 0.78, 1.5 and 3.1 kJ. The results were compared with the previous results for the contact surface and Mach disk. Results showed that the blast wave and contact surface moved together until about 50 μs after plasma initiation. Approximately 160 μs after plasma initiation the supersonic expansion has grown to its maximum downrange extension, and the barrel shock structure has been fully established. At later times the blast wave decouples from the driving core jet flow, and the constraint by the outer blast wave diminishes as the barrel shock retreats towards the capillary bore exit. The motion of the blast wave from a 5.0 kV (3.1 kJ) discharge, did not scale as expected for a strong shock ($\beta=0$) resulting from instantaneous energy deposition at a point. However, in accordance with the instantaneous point deposition model, the velocity of the blast wave scales as the square root of the dissipated energy ($E^{1/2}$) and shows maximum velocity (668 m/s) for the 3.1 kJ case.

Acknowledgements

One of the authors (J. U. Kim) would like to thank to Profs. N. Clemens and P. Varghese for their useful discussions.

References

Abbet, M., 1971, "Mach disk in Underexpanded Exhausted Plumes," *AIAA J.* Vol. 9, No. 3, pp. 512~514.

Christ, S., Sherman, P. M. and Glass, D. R., 1966, "Study of the Highly Underexpanded Sonic Jet," *AIAA J.* Vol. 4, No. 1, pp. 68~71.

Dabora, E. K., 1972, "Variable Energy Blast Waves," *AIAA J.* Vol. 10, No. 10, pp. 1384~1386.

Del Guercio, M., 1997, "Propellant Burn Rate Modification by Plasma Injection," *Proceeding of the 34th JANNAF Combustion Meeting*, CPIA Publication 662, Vol. 1, pp. 35~42.

Dyvik, J. A. and Katulka, G., 1996, "ETC Temperature Compensation; Experimental Results of 120-mm Test Firings," *Proceeding of the 33rd JANNAF Combustion Meeting*, CPIA Publication 653, Vol. 3, pp. 111~119.

Eggins, P. L. and Jackson, D. A., 1974, "Laser Doppler Velocity Measurements in an Under-Expanded Free Jet," *Journal of Physics D: Applied Physics*, Vol. 7, No. 14, pp. 1894~1906.

Gilligan, J., Bourham, M., Hankins, O., Aucillo, O., Tallavarjula, S. and Mohanti, R., 1991, "Studies to Reduce Material Erosion in Electrothermal Launchers," *IEEE Trans. Mag.*, Vol. 27, No. 1, pp. 476~481.

Greig, J. R., Earnhart, J. R., Winsor, N. K., McElroy, H. A., Juhasz, A. A., Wren, G. P. and Morrison, W. F., 1993, "Investigation of Plasma Augmented Solid Propellant Interior Ballistics Process," *IEEE Trans. Mag.*, Vol. 29, No. 1, pp. 555~560.

Hewkin, D. and Figura, E., 1993, "Fundamental Research and Numerical Modeling of the Internal Ballistics of Electrothermal Chemical Guns," *IEEE Trans. Mag.*, Vol. 29, No. 1, pp. 561~566.

Kaplan, Z., Saphire, D., Melnik, M., Gorelic, Z., Ashkenazy, J., Sudai, M., Kimhe, D., Melnik, D., Smith, S. and Juhasz, A., 1993, "Electrothermal Augmentation of a Solid Propellant Launcher," *IEEE Trans. Mag.*, Vol. 29, No. 1, pp. 573~578.

Kim, K. J. and Wilson, D. E., 1999, "Theoretical Analysis of a Plasma Jet Impinging on a Nonreacting Surface," Paper 99-0455, AIAA 37th Aerospace Sciences Meeting.

Klingenberg, G. and Heimerl, J. M., 1992, "Gun Muzzle Blast and Flash" Chap. 6. *Progress in Astronautics and Aeronautics* Vol. 139.

Knoepfel, H., 1970, *Pulsed High Magnetic Fields*, North-Holland, The Netherlands.

Kohel, J. M., Su, L. K., Clemens, N. T., and Varghese, P. L., 1999, "Emission Spectroscopic Measurements and Analysis of a Pulsed Plasma Jet," *IEEE Trans. Mag.*, Vol. 35, No. 1, pp. 201~206.

Liepmann, H. W. and Roschko, A., 1957, *Elements of Gas Dynamics*, 1st ed., Wiley, New York.

Sakurai, A., 1964, *Basic Development in Fluid Dynamics*, Academic Press, Vol. 1, pp. 309~375.

Schmidt, E. M. and Shear, D. D., 1975, "Optical Measurements of Muzzle Blast," *AIAA J.* Vol. 13, No. 8, pp. 1086~1091.

Taylor, G. I., 1950, "The formation of a Blast Wave by a Very Intense Explosion," *Proc. Royal Soc.* (London), A201, pp. 159~174.

Wilson, D. E., Kim, K. J. and Raja, L. L., 1999, "Theoretical Analysis of an External Pulsed Plasma Jet," *IEEE Trans. on Mag.*, Vol. 35, No. 1, pp. 228~231.